Environmental Science & Technology

pubs.acs.org/est

Article

Contribution of Atmospheric Oxygenated Organic Compounds to Particle Growth in an Urban Environment

Xiaohui Qiao, Chao Yan,* Xiaoxiao Li, YiShuo Guo, Rujing Yin, Chenjuan Deng, Chang Li, Wei Nie, Mingyi Wang, Runlong Cai, Dandan Huang, Zhe Wang, Lei Yao, Douglas R. Worsnop, Federico Bianchi, Yongchun Liu, Neil M. Donahue, Markku Kulmala, and Jingkun Jiang*

Cite This: *Environ. Sci. Technol.* 2021, 55, 13646−13656

Read Online

ACCESS | Metrics & More | Article Recommendations | Supporting Information

ABSTRACT: Gas-phase oxygenated organic molecules (OOMs) can contribute substantially to the growth of newly formed particles. However, the characteristics of OOMs and their contributions to particle growth rate are not well understood in urban areas, which have complex anthropogenic emissions and atmospheric conditions. We performed long-term measurement of gas-phase OOMs in urban Beijing during 2018−2019 using nitrate-based chemical ionization mass spectrometry. OOM concentrations showed clear seasonal variations, with the highest in the summer and the lowest in the winter. Correspondingly, calculated particle growth rates due to OOM condensation were highest in summer, followed by spring, autumn, and winter. One prominent feature of OOMs in this urban environment was a high fraction (~75%) of nitrogen-containing OOMs. These nitrogen-containing OOMs contributed only 50−60% of the total growth rate led by OOM condensation, owing to their slightly higher volatility than non-nitrate OOMs. By comparing the calculated condensation growth rates and the observed particle growth rates, we showed that sulfuric acid and its clusters are the main contributors to the growth of sub-3 nm particles, with OOMs significantly promoting the growth of 3−25 nm particles. In wintertime Beijing, however, there are missing contributors to the growth of particles above 3 nm, which remain to be further investigated.

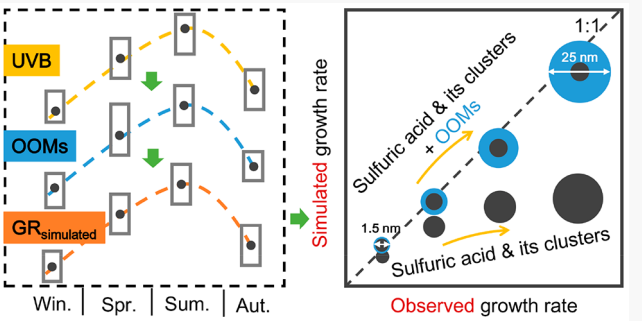

KEYWORDS: *oxygenated organic molecules, seasonal variation, particle growth, nitrogen-containing OOMs, urban environment*

1. INTRODUCTION

Atmospheric new particle formation (NPF) happens ubiquitously in various environments, and particles growing past a size of around 50 nm can be activated as cloud condensation nuclei (CCN), which influence cloud formation and climate.[1−3] NPF in polluted environments, despite the severe suppression by high aerosol loadings, has been shown to produce a large number of nanoparticles; these particles, if they survive scavenging by large existing particles, can grow and act as CCN.[4−6] Therefore, as a crucial determining factor for particle survival, particle growth rate can substantially influence the CCN budget.[7]

Condensable vapors, such as sulfuric acid, are important contributors to the growth of particles in various environments due to their low volatility.[8−10] Observations in Atlanta indicated that condensation of sulfuric acid and the subsequent equilibration with ammonia could substantially account for nanoparticle growth.[11] Also, it has been illustrated recently that condensation of H_2SO_4 and H_2SO_4-amine clusters contribute significantly to the growth of sub-3 nm particles in urban Beijing; however, sulfuric acid and its clusters alone cannot explain the growth of particles above 3 nm.[10] This is still far from "climate-relevant" size. There are still some missing contributors to particle growth, especially beyond the earliest stages.

Gas-phase oxygenated organic molecules (OOMs) are important for particle growth and even largely explain the particle growth rate in forested areas owing to their low volatility.[12−14] OOMs can be produced from the oxidation of volatile organic compounds (VOCs), including anthropogenic volatile organic compounds (AVOCs, e.g., benzene and toluene) and biogenic volatile organic compounds (BVOCs, e.g., isoprene, monoterpenes, and sesquiterpenes).[15−18] Chamber experiments have shown that the oxidation products of monoterpenes alone can trigger particle formation and drive the following growth.[19−22] Consistently, ambient observations

Received: March 31, 2021
Published: September 29, 2021

in a boreal forest in southern Finland (Hyytiälä) have shown that BVOC-derived OOMs are sufficient to explain particle growth over the size range of 3−50 nm.[13]

In contrast to remote forests, AVOCs are usually the dominant VOC species in urban environments, and NO_x levels are usually much higher. Thus, the characteristics of OOMs in polluted urban environments might be substantially different from those in forested areas. For BVOCs, auto-oxidation of RO_2 radicals is an important pathway of OOM formation.[14,18,23] Each auto-oxidation step results in an addition of two oxygen atoms, which greatly increases the oxygen number of OOMs.[16,24,25] For AVOCs, multigeneration oxidation is also an important pathway in OOMs formation.[26] This is mainly because the abundant NO_x in urban areas can suppress the auto-oxidation and terminate the chain propagation,[27] but also because the oxidation lifetime of later-generation AVOC products can be much lower than the precursor AVOCs.[28] As a result, OOMs generated under high NO_x conditions may have relatively higher volatilities than those in low NO_x conditions.[26,27,29] In wintertime Beijing, Yan et al.[30] demonstrated that OOMs are important for particle growth to CCN size. In another study in summertime Beijing, Brean et al.[31] showed that elevated OOM concentrations and particle growth coincided, implying an important contribution of OOMs to particle growth in urban areas. However, neither study had a quantitative evaluation of the contribution of OOMs to particle growth, and the contribution in different seasons has not been examined.

We conducted measurements of OOMs in urban Beijing during Jan. 2018 − Aug. 2019 covering four seasons. We investigated the overall characteristics of OOMs in urban Beijing in comparison to those in other atmospheric environments. We further evaluated the contribution of OOMs to particle growth over a size range of 1.5−25 nm and explored the dominant factors of its seasonal variation. Finally, we compared the calculated particle growth rates explained by sulfuric acid (including its clusters) and non-nitrogen/nitrogen-containing OOMs to the observed values.

2. METHODS

2.1. Measurements. The field measurements were conducted at an urban site located inside the west campus of Beijing University of Chemical Technology. The station is ∼500 m west to the Third Ring Road and is surrounded by residential and commercial areas. A detailed description about this site can be found in previous studies.[10,32] The measurements were between Jan. 2018 and Aug. 2019, covering all four seasons and including 27 NPF events with reliable OOMs and particle growth rate data in total. The exact duration of the four seasons are Mar. 3 to Apr. 7 2018 for spring with 5 NPF cases, Oct. 16 to Nov. 31 for autumn with 5 NPF cases, Jan. 25 to Feb. 6 and Dec. 10 to Dec. 24 2018 for winter with 11 NPF cases, and Jun. 15 to Aug. 31 2019 for summer with 6 NPF cases, respectively.

OOMs and H_2SO_4 were measured with nitrate-based chemical ionization atmospheric pressure interface time-of-flight mass spectrometers (CI-APi-ToF, Aerodyne Research Inc.).[33,34] A high-resolution time-of-flight mass spectrometer with the m/z resolution of ∼4000 Th/Th (CI-APi-HToF) was used in 2018, and a long time-of-flight mass spectrometer with the m/z resolution of ∼10 000 Th/Th (CI-APi-LToF) was used in 2019. Both instruments were calibrated for H_2SO_4 sensitivity and m/z-dependent transmission efficiency following previous studies.[20,35] Details of the sampling configurations are similar to those previously described.[10] In addition, H_2SO_4 clusters in this study refer to clusters containing up to four H_2SO_4 molecules and some base molecules as stabilizing agents. The concentration of these clusters was estimated using the simplified kinetic model described in Cai et al.[36]

Particle number concentrations and size distributions ranging from 1 nm to 10 μm were measured by a diethylene glycol scanning mobility particle spectrometer (DEG-SMPS; 1−7.5 nm)[37,38] together with a particle size distribution system (PSD; 3−10 μm).[39] A core sampling method was used in the DEG-SMPS system to achieve an aerosol sampling efficiency close to 100%.[40] A miniature cylindrical differential mobility analyzer (mini-cyDMA) was equipped for sub-10 nm aerosol classification and a modified DEG-UCPC with two-stage temperature control chamber was used for the front equipment for particle counting.[41] Meteorological data, including temperature, ambient pressure, wind speed, and wind direction, were measured with a local weather station (Vaisala, AWS310).

2.2. OOMs Quantification. OOM identification was performed with the tofTools package developed by Junninen et al.[42] The low background noises of the CI-APi-ToF are automatically removed in software. After obtaining the signals of assigned peaks, the concentrations of OOMs are calculated using eq 1:[20,35]

$$[\mathrm{OOM_i}] = C \times T_i \times \ln\left(1 + \frac{[\mathrm{OOM_i}\cdot \mathrm{NO_3^-}]}{\sum_{i=0}^{2}[(\mathrm{HNO_3})_i\cdot \mathrm{NO_3^-}]}\right) \quad (1)$$

Here, OOM signals in counts per second $[\mathrm{OOM_i}\cdot \mathrm{NO_3^-}]$ are normalized to the sum of reagent ion signals, including NO_3^-, $(HNO_3)NO_3^-$, and $(HNO_3)_2NO_3^-$. T_i is the mass-dependent transmission efficiency of the instrument, which was determined by adding different perfluorinated acid vapors in sufficient amounts to deplete NO_3^-.[35] C is the calibration coefficient obtained for H_2SO_4 using a homemade H_2SO_4 generator.[43] We conducted four calibrations during the observation period. The calibration coefficients are 4.79×10^9 and 4.5×10^9 $cm^{-3}\cdot cps^{-1}$ for CI-APi-HToF in 2018, 6.07×10^9 and 6.47×10^9 $cm^{-3}\cdot cps^{-1}$ for CI-APi-LToF in 2019. Here, we assume OOMs and H_2SO_4 have the same collision and binding efficiency with NO_3^-.[18] The charging efficiency for some less functionalized OOMs is likely lower than that for H_2SO_4, and therefore, the total OOM concentration measured by nitrate-based CI-APi-TOF should be regarded as a lower limit.

2.3. OOMs Volatility Estimation. Due to the lack of molecular structure information, OOM volatility was estimated using volatility parametrization methods based on the number of carbon, oxygen, and nitrogen atoms of the identified molecule.[44] As suggested by a recent study,[45] two volatility parametrization methods that treat OOMs with different functional groups were adopted in this study. One is for OOMs that mainly contain hydroperoxide groups, such as products via auto-oxidation:[13]

$$\log_{10} C^*_{300\mathrm{K}} = (25 - n_\mathrm{C})b_\mathrm{C} - (n_\mathrm{O} - 3n_\mathrm{N})b_\mathrm{O} - 2\frac{(n_\mathrm{O} - 3n_\mathrm{N})n_\mathrm{C}}{(n_\mathrm{C} + n_\mathrm{O} - 3n_\mathrm{N})}b_\mathrm{CO} - n_\mathrm{N}b_\mathrm{N} \quad (2)$$

where $b_C = 0.475$, $b_O = 0.2$, $b_{CO} = 0.9$, and $b_N = 2.5$, and n_C, n_O, and n_N are the number of carbon, oxygen, and nitrogen atoms in the compounds, respectively. The other is for OOMs that

https://doi.org/10.1021/acs.est.1c02095
Environ. Sci. Technol. 2021, 55, 13646−13656

mainly contain hydroxyl and carboxylic groups, such as products via multigeneration oxidation:[45]

$$\log_{10} C^*_{300K} = (25 - n_C)b_C - (n_O - 2n_N)b_O \quad (3)$$

where b_C = 0.475, and b_O = 2.3. A nitrate group reduces the similar extent of vapor pressure like a hydroxyl, and is replaced by hydroxyl for simplicity.[45] In terms of the oxidation pathway and the resulting functional groups, oxidation products of isoprene are also suitable for eq 3.[24] An empirical dividing line of H/C = −0.2*O/C + 1.5 is adopted in this study to separate OOMs with different kinds of main functional groups corresponding to the above two parametrization methods. The volatility of OOM above the line is estimated by eq 2, and otherwise by eq 3. More details about the volatility estimation method are available in the Supporting Information (SI).

OOMs measured by nitrate CI-APi-ToF are partly extremely low or low volatility organic compounds in Beijing (Figure S6). The oversaturated concentration of an OOM determines whether it can condense onto particulate matter or not. Due to the Kelvin effect, lower volatility is required for OOMs to condense onto smaller particles. According to the measured OOMs concentration in Beijing, OOMs with $\log_{10}(c^*) \geq 1$ could hardly condense on particles smaller than 25 nm (Figure S16). Therefore, we define OOMs with $\log_{10}(c^*) \leq 0$ as condensable OOMs, most of which are extremely low-volatility organic compounds (ELVOC, c^* in 10^{-8}–10^{-4} $\mu g \cdot m^3$) and low-volatility organic compounds (LVOC, c^* in 10^{-4}–10^{-1} $\mu g \cdot m^3$).[44]

2.4. Vapor Condensation Growth Rate Simulation. The condensation growth rate (GR), defined as GR = dd_p/dt, represents the change in particle size per unit time. The particle growth rate contributed by OOM condensation for a given diameter was calculated as eq 4,[19,46] and GR for a particle size bin is calculated by averaging the GR of all the particles in this bin.

$$\frac{dd_p}{dt} = \left(\frac{d_p + d_i}{d_p}\right)^2 \frac{\overline{c}_{i,p}}{2\rho} \alpha_{i,p} B_{i,p} [C_i^v - a_{i,p} C_i^0] \quad (4)$$

where d_p, d_i are the diameter of the particle and the condensable vapor, respectively; $\overline{c}_{i,p}$ is the mean relative thermal velocity between a condensable vapor molecular and a particle; ρ is the density of the particles; $\alpha_{i,p}$ is the accommodation coefficient; $B_{i,p}$ is the kinetic oriented transition-regime diffusion correction factor. The detailed calculations and assumptions of the above parameters are in the SI.

The square bracket term in eq 4 represents the driving force of OOM condensation, i.e., the oversaturated concentration of the condensable vapor. C_i^v and C_i^0 are the actual vapor concentration and saturation vapor concentration, respectively. $a_{i,p}$ is the particulate-phase activity, and $a_{i,p} = X_{i,p}\gamma_{i,p}K_{i,p}$, where $\gamma_{i,p}$ is the mass-based activity coefficient in the organic condensed phase, which is assumed to be 1. $K_{i,p}$ is the Kelvin coefficient, which is estimated by $K_{i,p} = 10^{d_{pK}/d_p}$. Assuming a particle surface tension of 0.034 $N \cdot m^{-1}$,[47,48] and a mean molar weight of 250 $g \cdot mol^{-1}$ at 300 K, the corresponding Kelvin diameter (d_{pK}) is 5 nm. $X_{i,p}$ is the mass fraction of OOM_i at the particle size of d_p. In this study, $X_{i,p}$ changes along with the growth of a new particle, and it was estimated by simulating the cumulative mass of OOM_i in the particulate phase based on the mass flux of OOM_i condensation.

The condensation growth rates contributed by H_2SO_4 and $(H_2SO_4)_n(DMA)_n$ are calculated following the method reported by Stolzenburg et al.,[9] which includes the effect of van der Waals forces in vapor condensation. The details of the calculation are supplemented in the SI.

It should be noted that the theoretical GR in eq 4 has a corresponding relationship with particle sizes (d_p) and time (t). For a particle size bin, e.g., 1.5–3 nm, the period used to calculate the theoretical $GR_{1.5-3}$ is consistent with that of observed $GR_{1.5-3}$ with log-normal distribution function method.[49] The time windows used for GR calculations are the exact periods when NPF events occur and develop. The criteria to identified NPF events and the calculation of observed GR is consistent with a previous study.[10]

3. RESULTS AND DISCUSSION

3.1. OOMs Observed in Urban Beijing. An overall of ~1100 organic formulas were identified within the m/z range of 200–450 Th for each season. The observed OOMs species in four seasons are generally similar in terms of the total number of identified molecules and the proportion of non-nitrogen OOM molecules (Figure S1). The mass-defect plot of the averaged OOMs in spring is shown in Figure 1 as an example.

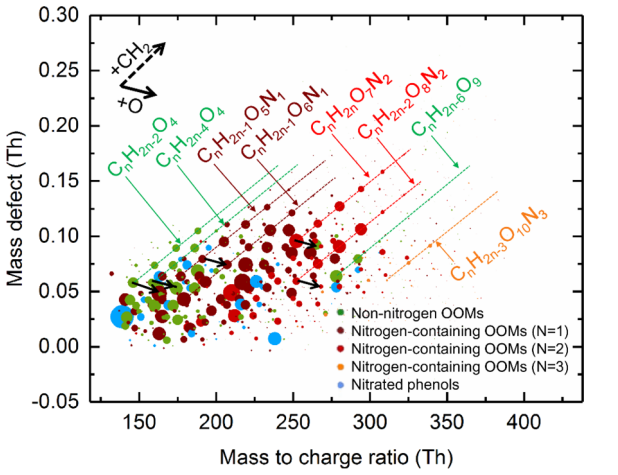

Figure 1. Mass-defect plot of observed oxygenated organic molecules (OOMs) in spring in Beijing. The detected OOMs are marked in the mass-defect plot by their exact mass and mass defect (exact mass subtracted by its unit mass). The differences in molecular composition are shown at regular spacing in the mass-defect plot. Adjacent points on the two direction lines differ by a $-CH_2-$ group or oxygen atom in composition. The general chemical formulas are annotated by the lines. OOMs with different numbers of nitrogen atoms are shown in different colors. Nitrated phenols are classified separately. The size of the circle corresponds to the concentration of OOMs.

Several groups of homologues were observed in both non-nitrogen OOMs and nitrogen-containing OOMs. Points aligned on the direction of $+CH_2$ are homologues, differing by an integral number of $-CH_2-$ group. The multiple series of homologous oxidation products are likely a result of the coexisting homologue precursors in urban areas, e.g., benzene, toluene, and xylene.[50]

Another important feature of OOMs in Beijing is the higher proportion of nitrogen-containing OOMs in comparison to that of forested area (Figures S2 and S3). In our measure-

https://doi.org/10.1021/acs.est.1c02095
Environ. Sci. Technol. 2021, 55, 13646−13656

ments, ~30% of the identified molecules are non-nitrogen OOMs and ~70% are nitrogen-containing OOMs. Among them, 35−52% of the total concentration of nitrogen-containing OOMs are OOMs with more than one nitrogen atom. The termination of auto-oxidation chain propagation by NO_x results in a carbonyl (RO_2 + NO reaction) or nitrate functional group (RO_2 + NO_x reaction).[14] Multigeneration oxidation of RO_2 + NO_x may explain the formation of OOMs with more than one nitrogen atom. Nitrate radical (NO_3) oxidation may also play a role. In addition to the high proportion of nitrogen-containing OOMs, strong auto-oxidation processes with more than two consecutive oxygen additions are rarely observed; this is consistent with NO_x reactions shortening RO_2 lifetimes in the urban environment.

Although the OOM speciation in each season is quite similar, the total concentration of OOMs in Beijing shows clear seasonal variations while falling within a similar range to concentrations observed elsewhere. As shown in Figure 2, the

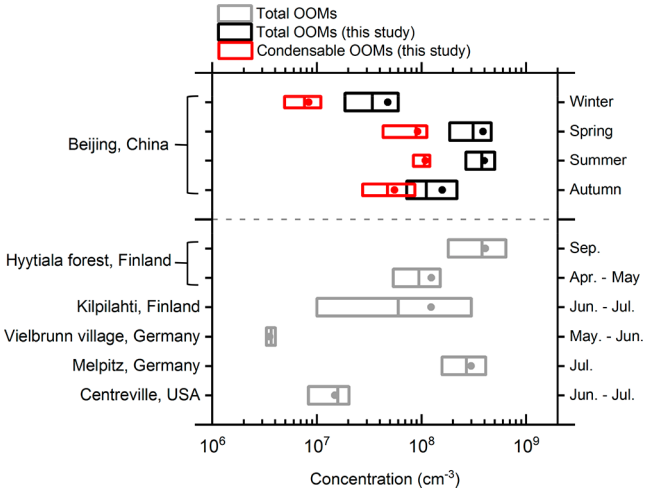

Figure 2. Comparison of atmospheric oxygenated organic molecules (OOMs) measured by nitrate CI-APi-ToF at different locations worldwide. Boxes in black and red are the results of total OOMs and condensable OOMs of urban Beijing during the whole observation periods in this study. Boxes in gray are previous results around the world, including Yan et al.[51] and Zha et al.[63] in Hyytiälä forest, Kürten et al.[64] in Vielbrunn village, Mutzel et al.[65] in Kilpilahti, Sarnela et al.[66] in Centreville, and Krechmer et al.[25] in Melpitz. Among them, Vielbrunn and Centreville only report the main oxidation products of monoterpene and isoprene, respectively. The boundaries of boxes on *x*-axis correspond to the 25th and 75th values. Lines and points in boxes are median and mean concentration, respectively.

seasonal median concentration of total OOMs in Beijing is the highest in summer (4.0×10^8 cm^{-3}), followed by spring (3.3×10^8 cm^{-3}), autumn (1.1×10^8 cm^{-3}), and winter (3.2×10^7 cm^{-3}). Similarly, the concentration of condensable OOMs in urban Beijing, accounting for 17−35% of total OOM concentration, also has the same seasonal variations. The high total OOM concentration in summer is most likely related to the enhanced photochemistry due to stronger solar radiation and higher temperature (Figure S8). From a global perspective, OOMs measured by nitrate CI-APi-ToF range from 10^7 to 10^9 cm^{-3}. It should be noted that nitrated phenols can contribute to 14−78% of the total OOM concentration in urban Beijing, which is higher than their contribution of ~16% in those remote forest areas.[51] However, as nitrated phenols are too volatile to have significant contribution to particle growth, they are excluded in the following discussion. The information on identified nitrated phenol peaks is supplemented in the SI.

The concentrations of both non-nitrogen OOMs and nitrogen-containing OOMs increase along with solar radiation (UVB) in the morning, which also coincides with particle growth processes. Such patterns are consistent during all four seasons (Figure S4). The averaged diurnal variations in summer are shown in Figure 3 as an example. Sulfuric acid

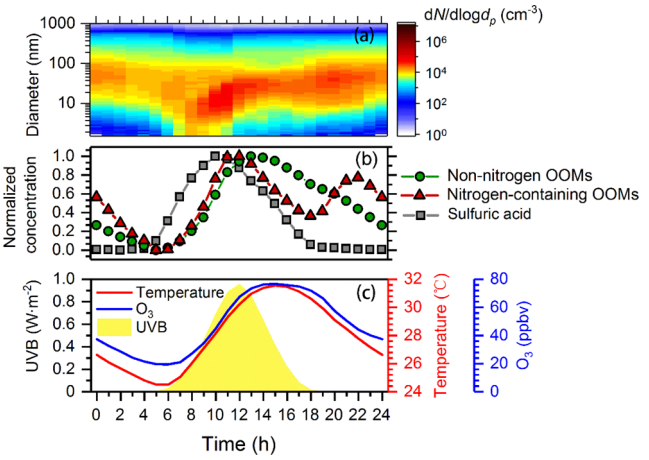

Figure 3. Diurnal variation of observed oxygenated organic compounds and other measured parameters in summer. Note that the particle size distribution shown in the top panel is the averaged result of new particle formation days.

starts to rise at around 5 am (local time) and reaches a peak at around 10 am. Both non-nitrogen OOMs and nitrogen-containing OOMs start to rise at 6 am; nitrogen-containing OOMs reach a peak at 11 am and non-nitrate OOMs reached the peak 1 h later. In daytime, OOMs increase along with the increase of solar radiation due to photochemistry, and decrease more slowly than sulfuric acid. This slower decrease of OOMs can be attributed to the continuing formation via ozone oxidation and the lower removal efficiency via condensation onto particles compared to sulfuric acid; this will be discussed in Section 3.2. In addition, the secondary peak of nitrogen-containing OOMs at around 10 pm may be due to the onset of NO_3 chemistry at nighttime.

3.2. Particle Growth Contributed by OOMs Condensation. The growth rates of 1.5−25 nm particles driven by condensation of OOMs are approximately 0.25−3.4 nm·h^{-1} and show clear seasonal variations. As shown in Figure 4, the condensation growth rates of OOMs, i.e., the sum of non-nitrate and nitrate OOMs, are the highest in summer, ranging from 1.7 to 3.4 nm·h^{-1}, followed by 0.7−2.0 nm·h^{-1} of spring, 0.96−1.48 nm·h^{-1} of autumn, and 0.25−0.3 nm·h^{-1} of winter. For particles in the same size range, the growth rates contributed by OOMs in summer can be 6.5−13 times those in winter. In addition, the contribution of nitrogen-containing OOMs to particle growth is larger than that of non-nitrogen OOMs in all size ranges and all four seasons, with calculated growth rates of 0.2−2.6 nm·h^{-1} and 0.05−0.9 nm·h^{-1}, respectively. Moreover, particle growth contributed by sulfuric acid and its clusters, nitrogen-containing OOMs, and non-nitrate OOMs have different size dependencies. With increasing particle diameter, the contribution by OOMs shows a flat or increasing trend, while the contribution by

https://doi.org/10.1021/acs.est.1c02095
Environ. Sci. Technol. 2021, 55, 13646−13656

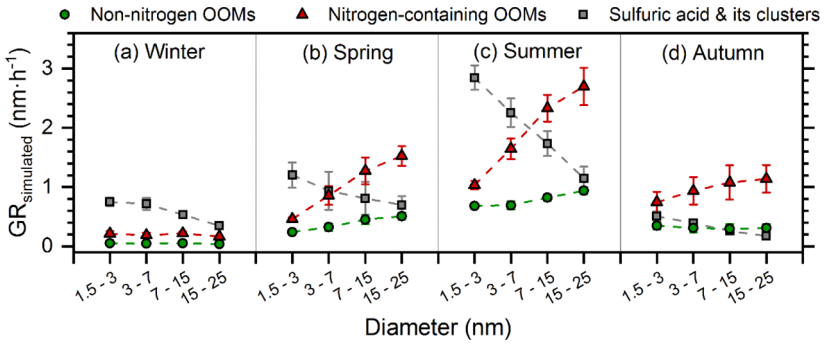

Figure 4. Simulated growth rates contributed by sulfuric acid and its clusters, non-nitrogen OOMs, and nitrogen-containing OOMs. Markers are the averaged results. Error bars are the standard deviations of the simulated results. There are 11, 5, 6, and 5 new particle cases for winter, spring, summer, and autumn, respectively. The particle growth period of each case (generally 7 am-12 pm) is used for simulation.

sulfuric acid considerably decreases. Taking summer as an example, from 1.5−3 nm to 15−25 nm, the contribution of sulfuric acid and its clusters decreased from 2.95 to 1.18 nm·h^{-1}, nitrogen-containing OOMs increased from 1.03 to 2.76 nm·h^{-1}, and non-nitrogen OOMs increased from 0.78 to 1.0 nm·h^{-1}.

The difference of condensation growth rates during four seasons is primarily due to the strong seasonal variation of the condensable OOM concentration. As shown in Figure 5a,b, the condensation growth rate contributed by OOMs correlated well (Pearson correlation coefficient of 0.95−0.99 in linear scale) with the condensable OOM concentration for each particle size range (Figure S10). This is because the volatility distributions of both non-nitrogen OOMs and nitrogen-containing OOMs are relatively stable in four seasons (Figure S11). Therefore, for any given particle size, the driving force of particle growth is almost solely determined by the gas-phase concentration of condensable OOMs. As shown in Figure 6, the concentrations of both non-nitrogen OOMs and nitrogen-containing OOMs vary by almost 1 order of magnitude, leading to a similar extent of variations in particle growth rate.

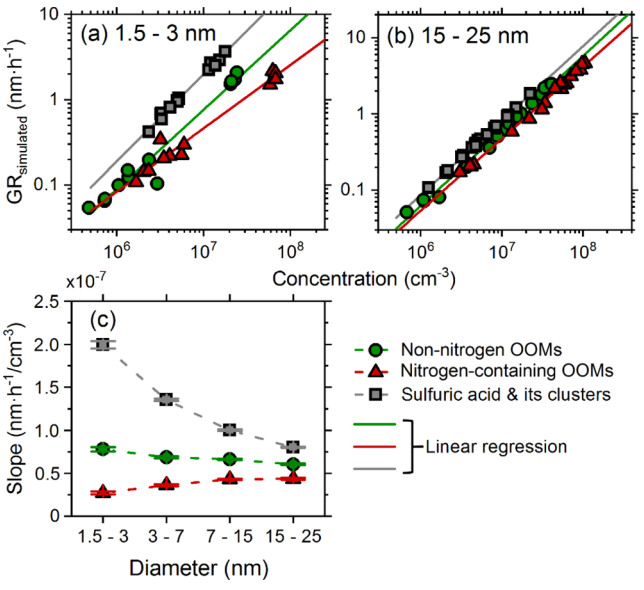

Figure 5. Growth promotion efficiency of different condensing vapors in condensation growth rate. (a, b) Vapor concentration and simulated condensation growth rate for different particle size bins, including sulfuric acid and its clusters, non-nitrogen OOMs, and nitrogen-containing OOMs. Solid lines are the linear regressions for different vapors. (c) Slopes of linear regressions ($GR_{simulated}$ vs concentration) for different particle size bins, including 1−3, 3−7, 7−15, and 15−25 nm. The green circle represents non-nitrogen OOMs, the red triangle represents nitrogen-containing OOMs, and the gray square represents sulfuric acid and its clusters. The caps of the markers in panel (c) are error bars for linear regression uncertainties, which range from 7.2×10^{-10} to 4.3×10^{-9} nm·h^{-1}/cm^{-3}.

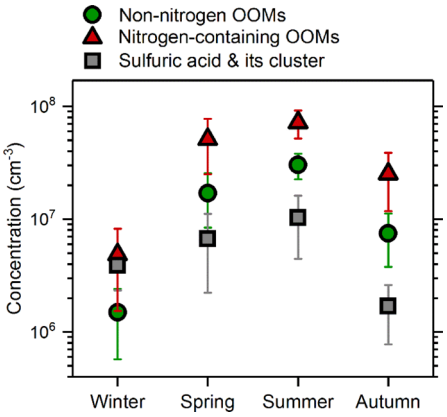

Figure 6. Concentrations of condensable oxygenated organic molecules (OOMs) in four seasons. Markers are the averaged results. Error bars are the standard deviations. The green circle represents non-nitrogen OOMs, the red triangle represents nitrogen-containing OOMs, and the gray square represents sulfuric acid and its clusters.

In addition to vapor concentration, the effectiveness of vapor condensation also influences the contribution of a certain gaseous species to particle growth. Here, we use the term "growth promotion efficiency (GPE)", defined as the resulting growth rate per unit concentration (e.g., nm·h^{-1}/cm^{-3}). From this perspective, sulfuric acid and its clusters are the most efficient condensable vapors, followed by non-nitrate OOMs and nitrogen-containing OOMs (Figure 5c). The GPE is essentially determined by the bulk volatility and the averaged molar mass of different species.[52] Sulfuric acid, although with a small molar mass, can hardly evaporate, so that it has the highest efficiency. For the case of OOMs, non-nitrogen OOMs and nitrogen-containing OOMs have similar molar mass, but the bulk volatility of non-nitrate OOMs is lower than that of nitrogen-containing OOMs (Figures S12 and S13). Therefore, the GPE of non-nitrate OOMs is higher than that of nitrogen-containing OOMs, and with the same vapor concentration,

https://doi.org/10.1021/acs.est.1c02095
Environ. Sci. Technol. 2021, 55, 13646−13656

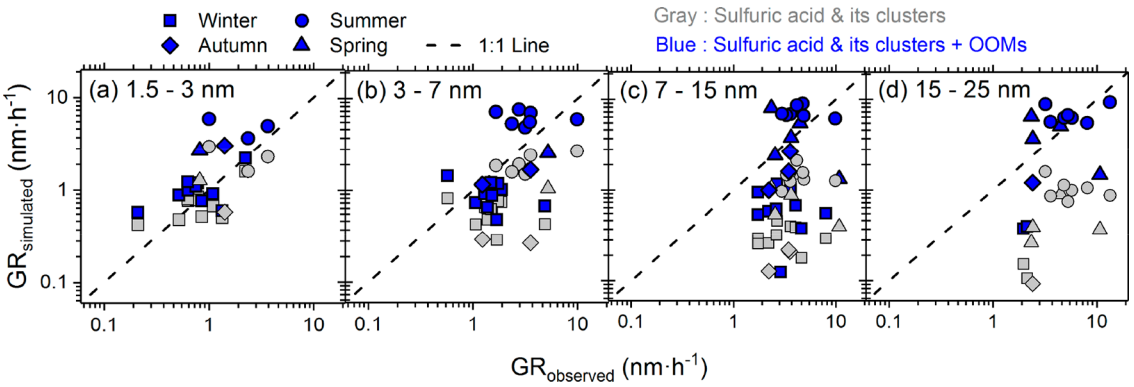

Figure 7. Relations of simulated growth rate and observed growth rate for different particle size bins. Results of different seasons are shown in different shapes of markers. The *x*-axis is the observed growth rate, and the *y*-axis is the simulated growth rate. The simulated growth rate of sulfuric acid and its clusters are shown in gray, and the blue ones are sulfuric acid and its clusters plus OOMs. The dashed lines are 1:1 lines. Note that the observed growth rates are calculated using mode fitting method.

non-nitrate OOMs lead to larger growth rates than nitrogen-containing OOMs do.

Taking both the vapor concentration and GPE into consideration, we could explain the difference of condensation growth rate between non-nitrogen OOMs and nitrogen-containing OOMs. The total concentrations of condensable nitrogen-containing OOMs are 2.67−3.37 times those of non-nitrogen OOMs (Figure 6), but the lower GPE of nitrogen-containing OOMs (Figure 5c) partially offsets the higher concentration. As a whole, the growth rates contributed by nitrogen-containing OOMs are 1−2.33 times that by non-nitrogen OOMs.

As also shown in Figure 5c, the GPE of different species varies differently across particle sizes. For sulfuric acid and its clusters, their GPE decrease with increased particle sizes. This is because condensation of the same amount of sulfuric acid causes smaller increases in diameters for large particles than for small particles. A similar effect is expected for OOMs, however, OOM condensation is also strongly influenced by the Kelvin effect. More OOMs can condense as particles grow larger and the Kelvin effect diminishes, which compensates for the size effect and leads to an overall weak size dependence.

4. ATMOSPHERIC IMPLICATIONS

This study reports the seasonal characteristics of OOMs in an urban environment and supplements for the global scheme,[14] which helps to better understand OOMs formation in different environments. We found an atmospheric relevance between solar radiation and OOMs concentration in a seasonal scale: with the increase of solar radiation intensity (from winter to summer), the concentration of day-time OOMs rises rapidly first and then increases slowly (Figure S8a). The strength of solar radiation is correlated with OH radical concentration and atmospheric temperature.[53,54] Since the concentration of precursors in winter is not significantly lower than other seasons (Figure S9a) and its loss through condensation sink is not higher than other seasons (Figure S9c), the lower oxidant concentrations (e.g., OH radical) and lower temperature may substantially limit the formation of OOMs in wintertime. Compared with the seasonal variations of VOC precursors and condensation sink, photochemical strength seems to play a more important role in the seasonal variation of OOM concentrations based on its better consistency (Figure S9). This correlation may also exist in other midlatitude urban and forested environments that have distinct seasonal changes.

In urban Beijing, sulfuric acid and its clusters can explain a significant fraction of the observed growth of 1.5−3 nm particles,[10] and OOMs have a significant contribution to the growth of 3−25 nm particles (Figure 7). The higher contribution of sulfuric acid and its clusters in 1.5−3 nm particles can be explained by their high GPE at this size range (Figure 5c). In addition, the concentration of sulfuric acid rises early and steeply during the time window when the initial growth of new particles occurs (Figure 3). For larger (3−25 nm) particles, despite the lower GPE of OOMs compared to sulfuric acid, OOMs start to dominate particle growth, due to the much higher vapor concentration and the increasingly weaker Kelvin effect. Overall, the contributions by sulfuric acid and OOMs can explain a major fraction of the observed growth rate in all size ranges of 1.5−25 nm.

It was reported that NPF events in Beijing can contribute to the surface area concentration and mass concentration of atmospheric aerosols (mainly governed by particles larger than 100 nm), especially under conditions with a fast growth of newly formed particles.[5,55] Although this study focused on the growth of nanoparticles, the condensation of OOMs is expected to contribute significantly to the growth of large particles as well.

However, winter is an exception. A clear discrepancy remains between the simulated and observed growth rate in 3−25 nm particles, which may be an indication of some missing contributors. One plausible cause is the underestimation of condensable OOM concentration at low temperatures. Nitrate CI-APi-ToF is less sensitive to moderately oxidized molecules,[56] while with the decrease of temperature, some moderately oxidized organics may become condensable and contribute to particle growth.[57] Meanwhile, particle-phase processes could promote particle growth through lowering the volatility of particle-phase organics,[58] including condensed phase reactions and oligomerization.[59] Another possible reason is the missing contributions by inorganic compounds as suggested by recent chamber studies, e.g., HNO_3 and NH_3 at low temperatures,[60] HIO_3 with high ambient concentration.[61]

In some cases, the simulated particle growth rates are higher than observed values (Figure 7). This may arise from two sources of uncertainties. One is the uncertainty in growth rate

https://doi.org/10.1021/acs.est.1c02095
Environ. Sci. Technol. 2021, 55, 13646−13656

simulation, which mainly comes from the estimation of OOMs volatility (Figure S5). The other is from the calculation of observed growth rate. As illustrated by Deng et al.,[10] growth rates calculated using the appearance time method and the log-normal distribution method can sometimes differ by a factor of 2. We investigated the results of appearance time growth rate and corrected the influence by particle coagulation[62] (Figures S14 and S15). The ratios of simulated growth rate over observed growth rate are lower when the particle growth rates are calculated with the appearance time method. However, our findings on the important role of OOMs in explaining the growth rate of 3−25 nm particles remain valid. In addition, the sum of OOMs, sulfuric acid, and its clusters is still far from explaining the observed growth rate (appearance time method) in winter.

■ ASSOCIATED CONTENT

Supporting Information

The Supporting Information is available free of charge at https://pubs.acs.org/doi/10.1021/acs.est.1c02095.

Detailed information on the calculation method of simulated growth rate; Figure S1, comparison of observed oxygenated organic molecules in all of the four seasons using Venn plot; Figures S2 and S3, proportion of carbon-resolved non-nitrogen OOMs and nitrogen-containing OOMs in Beijing and other atmospheric environment; Figure S4, diurnal variation of sulfuric acid, non-nitrogen OOMs, and nitrogen-containing OOMs in all four seasons; Figure S5, comparison of two volatility parametrization methods; Figure S6, the volatility distribution of observed OOMs in Beijing for four seasons; Figure S7, relations between H to C ratio and O to C ratio of known OOMs peaklists from laboratory studies; Figure S8, relations of condensable oxygenated organic molecules with temperature and solar radiation; Figure S9, seasonal variations of volatile organic compounds, temperature and solar radiation, and CS in Beijing; Figure S10, relations of size-resolved simulated growth rate and condensing vapor concentration; Figure S11, relations of driving force and OOMs concentration; Figure S12, growth efficiency of different kinds of condensing vapors; Figure S13, volatility distribution of non-nitrogen OOMs and nitrogen-containing OOMs; Figures S14 and S15, relations of simulated GR and observed GR (appearance time method) for different particle size bins; Figure S16, the condensation growth rate contributed by OOMs with different volatilities for 1.5−25 nm particles; Figure S17, six examples for peak identification in tofTool; Figure S18, concentration of total OOMs in NPF days and non-NPF days; and Table S1, identified nitrated phenol peaks during the measurement (PDF)

■ AUTHOR INFORMATION

Corresponding Authors

Jingkun Jiang − *State Key Joint Laboratory of Environment Simulation and Pollution Control, School of Environment, Tsinghua University, 100084 Beijing, P. R. China;* orcid.org/0000-0001-6172-190X; Email: jiangjk@tsinghua.edu.cn

Chao Yan − *Institute for Atmospheric and Earth System Research/Physics, Faculty of Science, University of Helsinki, 00014 Helsinki, Finland; Aerosol and Haze Laboratory, Beijing Advanced Innovation Center for Soft Matter Science and Engineering, Beijing University of Chemical Technology, 100029 Beijing, P. R. China;* Email: chao.yan@helsinki.fi

Authors

Xiaohui Qiao − *State Key Joint Laboratory of Environment Simulation and Pollution Control, School of Environment, Tsinghua University, 100084 Beijing, P. R. China*

Xiaoxiao Li − *State Key Joint Laboratory of Environment Simulation and Pollution Control, School of Environment, Tsinghua University, 100084 Beijing, P. R. China;* orcid.org/0000-0002-0376-2460

YiShuo Guo − *Aerosol and Haze Laboratory, Beijing Advanced Innovation Center for Soft Matter Science and Engineering, Beijing University of Chemical Technology, 100029 Beijing, P. R. China*

Rujing Yin − *State Key Joint Laboratory of Environment Simulation and Pollution Control, School of Environment, Tsinghua University, 100084 Beijing, P. R. China*

Chenjuan Deng − *State Key Joint Laboratory of Environment Simulation and Pollution Control, School of Environment, Tsinghua University, 100084 Beijing, P. R. China*

Chang Li − *Aerosol and Haze Laboratory, Beijing Advanced Innovation Center for Soft Matter Science and Engineering, Beijing University of Chemical Technology, 100029 Beijing, P. R. China*

Wei Nie − *Joint International research Laboratory of Atmospheric and Earth System Research, School of Atmospheric Sciences, Nanjing University, Nanjing 210023, P. R. China;* orcid.org/0000-0002-6048-0515

Mingyi Wang − *Center for Atmospheric Particle Studies, Carnegie Mellon University, Pittsburgh, Pennsylvania 15213, United States;* orcid.org/0000-0001-5782-2513

Runlong Cai − *Institute for Atmospheric and Earth System Research/Physics, Faculty of Science, University of Helsinki, 00014 Helsinki, Finland; Aerosol and Haze Laboratory, Beijing Advanced Innovation Center for Soft Matter Science and Engineering, Beijing University of Chemical Technology, 100029 Beijing, P. R. China*

Dandan Huang − *State Environmental Protection Key Laboratory of Formation and Prevention of Urban Air Pollution Complex, Shanghai Academy of Environmental Sciences, Shanghai 200233, P. R. China;* orcid.org/0000-0003-2878-7469

Zhe Wang − *Division of Environment and Sustainability, The Hong Kong University of Science and Technology, Hong Kong SAR 999077, P. R. China;* orcid.org/0000-0002-5627-6562

Lei Yao − *Institute for Atmospheric and Earth System Research/Physics, Faculty of Science, University of Helsinki, 00014 Helsinki, Finland;* orcid.org/0000-0002-2680-1629

Douglas R. Worsnop − *Institute for Atmospheric and Earth System Research/Physics, Faculty of Science, University of Helsinki, 00014 Helsinki, Finland; Aerodyne Research Incoporated, Billerica, Massachusetts 01821, United States*

Federico Bianchi − *Institute for Atmospheric and Earth System Research/Physics, Faculty of Science, University of Helsinki, 00014 Helsinki, Finland; Aerosol and Haze Laboratory, Beijing Advanced Innovation Center for Soft Matter Science and Engineering, Beijing University of*

Chemical Technology, 100029 Beijing, P. R. China; orcid.org/0000-0003-2996-3604

Yongchun Liu − *Aerosol and Haze Laboratory, Beijing Advanced Innovation Center for Soft Matter Science and Engineering, Beijing University of Chemical Technology, 100029 Beijing, P. R. China;* orcid.org/0000-0002-9055-970X

Neil M. Donahue − *Center for Atmospheric Particle Studies and Department of Chemistry, Carnegie Mellon University, Pittsburgh, Pennsylvania 15213, United States*

Markku Kulmala − *Institute for Atmospheric and Earth System Research/Physics, Faculty of Science, University of Helsinki, 00014 Helsinki, Finland; Aerosol and Haze Laboratory, Beijing Advanced Innovation Center for Soft Matter Science and Engineering, Beijing University of Chemical Technology, 100029 Beijing, P. R. China*

Complete contact information is available at: https://pubs.acs.org/10.1021/acs.est.1c02095

Notes

The authors declare no competing financial interest.

■ ACKNOWLEDGMENTS

Financial support from the National Science Foundation of China (92044301, 21876094, and 41730106) and Samsung $PM_{2.5}$ SRP are acknowledged.

■ REFERENCES

(1) Kulmala, M.; Vehkamäki, H.; Petäjä, T.; Dal Maso, M.; Lauri, A.; Kerminen, V. M.; Birmili, W.; McMurry, P. H. Formation and growth rates of ultrafine atmospheric particles: A review of observations. *J. Aerosol Sci.* **2004**, *35*, 143−176.

(2) Kerminen, V. M.; Lihavainen, H.; Komppula, M.; Viisanen, Y.; Kulmala, M. Direct observational evidence linking atmospheric aerosol formation and cloud droplet activation. *Geophys. Res. Lett.* **2005**, *32*, 1−4.

(3) Merikanto, J.; Spracklen, D. V.; Mann, G. W.; Pickering, S. J.; Carslaw, K. S. Impact of nucleation on global CCN. *Atmos. Chem. Phys.* **2009**, *9*, 8601−8616.

(4) McMurry, P. H.; Friedlander, S. K. New particle formation in the presence of an aerosol. *Atmos. Environ.* **1979**, *13* (12), 1635−1651.

(5) Guo, S.; Hu, M.; Zamora, M. L.; Peng, J.; Shang, D.; Zheng, J.; Du, Z.; Wu, Z.; Shao, M.; Zeng, L.; Molina, M. J.; Zhang, R. Elucidating severe urban haze formation in China. *Proc. Natl. Acad. Sci. U. S. A.* **2014**, *111*, 17373−17378.

(6) Cai, R. L.; Yang, D. S.; Fu, Y. Y.; Wang, X.; Li, X. X.; Ma, Y.; Hao, J. M.; Zheng, J.; Jiang, J. K. Aerosol surface area concentration: a governing factor in new particle formation in Beijing. *Atmos. Chem. Phys.* **2017**, *17* (20), 12327−12340.

(7) Kulmala, M.; Kerminen, V. M.; Petäjä, T.; Ding, A. J.; Wang, L. Atmospheric gas-to-particle conversion: Why NPF events are observed in megacities? *Faraday Discuss.* **2017**, *200*, 271−288.

(8) McMurry, P. H.; Fink, M.; Sakurai, H.; Stolzenburg, M. R.; Mauldin, I. L.; Smith, J.; Eisele, F.; Moore, K.; Sjostedt, S.; Tanner, D.; Huey, L. G.; Nowak, J. B.; Edgerton, E.; Voisin, D. A criterion for new particle formation in the sulfur-rich Atlanta atmosphere. *J. Geophys. Res.* **2005**, *110*, 1−10.

(9) Stolzenburg, D.; Simon, M.; Ranjithkumar, A.; Kürten, A.; Lehtipalo, K.; Gordon, H.; Ehrhart, S.; Finkenzeller, H.; Pichelstorfer, L.; Nieminen, T.; He, X.-C.; Brilke, S.; Xiao, M.; Amorim, A.; Baalbaki, R.; Baccarini, A.; Beck, L.; Bräkling, S.; Caudillo Murillo, L.; Chen, D.; Chu, B.; Dada, L.; Dias, A.; Dommen, J.; Duplissy, J.; El Haddad, I.; Fischer, L.; Gonzalez Carracedo, L.; Heinritzi, M.; Kim, C.; Koenig, T. K.; Kong, W.; Lamkaddam, H.; Lee, C. P.; Leiminger, M.; Li, Z.; Makhmutov, V.; Manninen, H. E.; Marie, G.; Marten, R.; Müller, T.; Nie, W.; Partoll, E.; Petäjä, T.; Pfeifer, J.; Philippov, M.; Rissanen, M. P.; Rörup, B.; Schobesberger, S.; Schuchmann, S.; Shen, J.; Sipilä, M.; Steiner, G.; Stozhkov, Y.; Tauber, C.; Tham, Y. J.; Tomé, A.; Vazquez-Pufleau, M.; Wagner, A. C.; Wang, M.; Wang, Y.; Weber, S. K.; Wimmer, D.; Wlasits, P. J.; Wu, Y.; Ye, Q.; Zauner-Wieczorek, M.; Baltensperger, U.; Carslaw, K. S.; Curtius, J.; Donahue, N. M.; Flagan, R. C.; Hansel, A.; Kulmala, M.; Lelieveld, J.; Volkamer, R.; Kirkby, J.; Winkler, P. M. Enhanced growth rate of atmospheric particles from sulfuric acid. *Atmos. Chem. Phys.* **2020**, *20* (12), 7359−7372.

(10) Deng, C.; Fu, Y.; Dada, L.; Yan, C.; Cai, R.; Yang, D.; Zhou, Y.; Yin, R.; Lu, Y.; Li, X.; Qiao, X.; Fan, X.; Nie, W.; Kontkanen, J.; Kangasluoma, J.; Chu, B.; Ding, A.; Kerminen, V. M.; Paasonen, P.; Worsnop, D. R.; Bianchi, F.; Liu, Y.; Zheng, J.; Wang, L.; Kulmala, M.; Jiang, J. Seasonal Characteristics of New Particle Formation and Growth in Urban Beijing. *Environ. Sci. Technol.* **2020**, *54* (14), 8547−8557.

(11) Stolzenburg, M. R.; McMurry, P. H.; Sakurai, H.; Smith, J. N.; Mauldin, R. L.; Eisele, F. L.; Clement, C. F. Growth rates of freshly nucleated atmospheric particles in Atlanta. *J. Geophys. Res.* **2005**, *110*, 1−10.

(12) Riipinen, I.; Yli-Juuti, T.; Pierce, J. R.; Petäjä, T.; Worsnop, D. R.; Kulmala, M.; Donahue, N. M. The contribution of organics to atmospheric nanoparticle growth. *Nat. Geosci.* **2012**, *5*, 453−458.

(13) Mohr, C.; Thornton, J. A.; Heitto, A.; Lopez-Hilfiker, F. D.; Lutz, A.; Riipinen, I.; Hong, J.; Donahue, N. M.; Hallquist, M.; Petäjä, T.; Kulmala, M.; Yli-Juuti, T. Molecular identification of organic vapors driving atmospheric nanoparticle growth. *Nat. Commun.* **2019**, *10*, 1−7.

(14) Bianchi, F.; Kurten, T.; Riva, M.; Mohr, C.; Rissanen, M. P.; Roldin, P.; Berndt, T.; Crounse, J. D.; Wennberg, P. O.; Mentel, T. F.; Wildt, J.; Junninen, H.; Jokinen, T.; Kulmala, M.; Worsnop, D. R.; Thornton, J. A.; Donahue, N.; Kjaergaard, H. G.; Ehn, M. Highly Oxygenated Organic Molecules (HOM) from Gas-Phase Autoxidation Involving Peroxy Radicals: A Key Contributor to Atmospheric Aerosol. *Chem. Rev.* **2019**, *119* (6), 3472−3509.

(15) Molteni, U.; Bianchi, F.; Klein, F.; El Haddad, I.; Frege, C.; Rossi, M. J.; Dommen, J.; Baltensperger, U. Formation of highly oxygenated organic molecules from aromatic compounds. *Atmos. Chem. Phys.* **2018**, *18*, 1909−1921.

(16) Jokinen, T.; Kausiala, O.; Garmash, O.; Peräkylä, O.; Junninen, H.; Schobesberger, S.; Yan, C.; Sipilä, M.; Rissanen, M. P. Production of highly oxidized organic compounds from ozonolysis of β-caryophyllene: Laboratory and field measurements. *Boreal Environment Research* **2016**, *21*, 262−273.

(17) Lee, A.; Goldstein, A. H.; Kroll, J. H.; Ng, N. L.; Varutbangkul, V.; Flagan, R. C.; Seinfeld, J. H. Gas-phase products and secondary aerosol yields from the photooxidation of 16 different terpenes. *J. Geophys. Res.* **2006**, *111*, 1−25.

(18) Ehn, M.; Thornton, J. A.; Kleist, E.; Sipila, M.; Junninen, H.; Pullinen, I.; Springer, M.; Rubach, F.; Tillmann, R.; Lee, B.; Lopez-Hilfiker, F.; Andres, S.; Acir, I. H.; Rissanen, M.; Jokinen, T.; Schobesberger, S.; Kangasluoma, J.; Kontkanen, J.; Nieminen, T.; Kurten, T.; Nielsen, L. B.; Jorgensen, S.; Kjaergaard, H. G.; Canagaratna, M.; Maso, M. D.; Berndt, T.; Petaja, T.; Wahner, A.; Kerminen, V. M.; Kulmala, M.; Worsnop, D. R.; Wildt, J.; Mentel, T. F. A large source of low-volatility secondary organic aerosol. *Nature* **2014**, *506*, 476−479.

(19) Tröstl, J.; Chuang, W. K.; Gordon, H.; Heinritzi, M.; Yan, C.; Molteni, U.; Ahlm, L.; Frege, C.; Bianchi, F.; Wagner, R.; Simon, M.; Lehtipalo, K.; Williamson, C.; Craven, J. S.; Duplissy, J.; Adamov, A.; Almeida, J.; Bernhammer, A. K.; Breitenlechner, M.; Brilke, S.; Dias, A.; Ehrhart, S.; Flagan, R. C.; Franchin, A.; Fuchs, C.; Guida, R.; Gysel, M.; Hansel, A.; Hoyle, C. R.; Jokinen, T.; Junninen, H.; Kangasluoma, J.; Keskinen, H.; Kim, J.; Krapf, M.; Kurten, A.; Laaksonen, A.; Lawler, M.; Leiminger, M.; Mathot, S.; Mohler, O.; Nieminen, T.; Onnela, A.; Petaja, T.; Piel, F. M.; Miettinen, P.; Rissanen, M. P.; Rondo, L.; Sarnela, N.; Schobesberger, S.; Sengupta, K.; Sipila, M.; Smith, J. N.; Steiner, G.; Tome, A.; Virtanen, A.; Wagner, A. C.; Weingartner, E.; Wimmer, D.; Winkler, P. M.; Ye, P.;

Carslaw, K. S.; Curtius, J.; Dommen, J.; Kirkby, J.; Kulmala, M.; Riipinen, I.; Worsnop, D. R.; Donahue, N. M.; Baltensperger, U. The role of low-volatility organic compounds in initial particle growth in the atmosphere. *Nature* **2016**, *533* (7604), 527−31.

(20) Kirkby, J.; Duplissy, J.; Sengupta, K.; Frege, C.; Gordon, H.; Williamson, C.; Heinritzi, M.; Simon, M.; Yan, C.; Almeida, J.; Trostl, J.; Nieminen, T.; Ortega, I. K.; Wagner, R.; Adamov, A.; Amorim, A.; Bernhammer, A. K.; Bianchi, F.; Breitenlechner, M.; Brilke, S.; Chen, X.; Craven, J.; Dias, A.; Ehrhart, S.; Flagan, R. C.; Franchin, A.; Fuchs, C.; Guida, R.; Hakala, J.; Hoyle, C. R.; Jokinen, T.; Junninen, H.; Kangasluoma, J.; Kim, J.; Krapf, M.; Kurten, A.; Laaksonen, A.; Lehtipalo, K.; Makhmutov, V.; Mathot, S.; Molteni, U.; Onnela, A.; Perakyla, O.; Piel, F.; Petaja, T.; Praplan, A. P.; Pringle, K.; Rap, A.; Richards, N. A.; Riipinen, I.; Rissanen, M. P.; Rondo, L.; Sarnela, N.; Schobesberger, S.; Scott, C. E.; Seinfeld, J. H.; Sipila, M.; Steiner, G.; Stozhkov, Y.; Stratmann, F.; Tome, A.; Virtanen, A.; Vogel, A. L.; Wagner, A. C.; Wagner, P. E.; Weingartner, E.; Wimmer, D.; Winkler, P. M.; Ye, P.; Zhang, X.; Hansel, A.; Dommen, J.; Donahue, N. M.; Worsnop, D. R.; Baltensperger, U.; Kulmala, M.; Carslaw, K. S.; Curtius, J. Ion-induced nucleation of pure biogenic particles. *Nature* **2016**, *533*, 521−526.

(21) Schobesberger, S.; Junninen, H.; Bianchi, F.; Lonn, G.; Ehn, M.; Lehtipalo, K.; Dommen, J.; Ehrhart, S.; Ortega, I. K.; Franchin, A.; Nieminen, T.; Riccobono, F.; Hutterli, M.; Duplissy, J.; Almeida, J.; Amorim, A.; Breitenlechner, M.; Downard, A. J.; Dunne, E. M.; Flagan, R. C.; Kajos, M.; Keskinen, H.; Kirkby, J.; Kupc, A.; Kurten, A.; Kurten, T.; Laaksonen, A.; Mathot, S.; Onnela, A.; Praplan, A. P.; Rondo, L.; Santos, F. D.; Schallhart, S.; Schnitzhofer, R.; Sipila, M.; Tome, A.; Tsagkogeorgas, G.; Vehkamaki, H.; Wimmer, D.; Baltensperger, U.; Carslaw, K. S.; Curtius, J.; Hansel, A.; Petaja, T.; Kulmala, M.; Donahue, N. M.; Worsnop, D. R. Molecular understanding of atmospheric particle formation from sulfuric acid and large oxidized organic molecules. *Proc. Natl. Acad. Sci. U. S. A.* **2013**, *110* (43), 17223−8.

(22) Zhao, J.; Ortega, J.; Chen, M.; McMurry, P. H.; Smith, J. N. Dependence of particle nucleation and growth on high molecular weight gas phase products during ozonolysis of α-pinene. *Atmos. Chem. Phys.* **2013**, *13*, 7631−7644.

(23) Crounse, J. D.; Nielsen, L. B.; Jørgensen, S.; Kjaergaard, H. G.; Wennberg, P. O. Autoxidation of organic compounds in the atmosphere. *J. Phys. Chem. Lett.* **2013**, *4*, 3513−3520.

(24) Wang, S.; Riva, M.; Yan, C.; Ehn, M.; Wang, L. Primary Formation of Highly Oxidized Multifunctional Products in the OH-Initiated Oxidation of Isoprene: A Combined Theoretical and Experimental Study. *Environ. Sci. Technol.* **2018**, *52*, 12255−12264.

(25) Krechmer, J. E.; Coggon, M. M.; Massoli, P.; Nguyen, T. B.; Crounse, J. D.; Hu, W.; Day, D. A.; Tyndall, G. S.; Henze, D. K.; Rivera-Rios, J. C.; Nowak, J. B.; Kimmel, J. R.; Mauldin, R. L., 3rd; Stark, H.; Jayne, J. T.; Sipila, M.; Junninen, H.; St Clair, J. M.; Zhang, X.; Feiner, P. A.; Zhang, L.; Miller, D. O.; Brune, W. H.; Keutsch, F. N.; Wennberg, P. O.; Seinfeld, J. H.; Worsnop, D. R.; Jimenez, J. L.; Canagaratna, M. R. Formation of Low Volatility Organic Compounds and Secondary Organic Aerosol from Isoprene Hydroxyhydroperoxide Low-NO Oxidation. *Environ. Sci. Technol.* **2015**, *49* (17), 10330−10339.

(26) Garmash, O.; Rissanen, M. P.; Pullinen, I.; Schmitt, S.; Kausiala, O.; Tillmann, R.; Zhao, D.; Percival, C.; Bannan, T. J.; Priestley, M.; Hallquist, A. M.; Kleist, E.; Kiendler-Scharr, A.; Hallquist, M.; Berndt, T.; McFiggans, G.; Wildt, J.; Mentel, T. F.; Ehn, M. Multi-generation OH oxidation as a source for highly oxygenated organic molecules from aromatics. *Atmos. Chem. Phys.* **2020**, *20*, 515−537.

(27) Rissanen, M. P. NO2 Suppression of Autoxidation-Inhibition of Gas-Phase Highly Oxidized Dimer Product Formation. *ACS Earth and Space Chemistry* **2018**, *2*, 1211−1219.

(28) Xiao, M.; Hoyle, C.; Dada, L.; Stolzenburg, D.; Kürten, A.; Wang, M.; Lamkaddam, H.; Garmash, O.; Mentler, B.; Molteni, U.; Baccarini, A.; Simon, M.; He, X.-C.; Lehtipalo, K.; Ahonen, L.; Baalbaki, R.; Bauer, P.; Beck, L.; Bell, D.; Bianchi, F.; Brilke, S.; Chen, D.; Chiu, R.; Dias, A.; Duplissy, J.; Finkenzeller, H.; Gordon, H.; Hofbauer, V.; Kim, C.; Koenig, T.; Lampilahti, J.; Lee, C. P.; Li, Z.; Mai, H.; Makhmutov, V.; Manninen, H.; Marten, R.; Mathot, S.; Mauldin, R.; Nie, W.; Onnela, A.; Partoll, E.; Petäjä, T.; Pfeifer, J.; Pospisilova, V.; Quéléver, L.; Rissanen, M.; Schobesberger, S.; Schuchmann, S.; Stozhkov, Y.; Tauber, C.; Tham, Y. J.; Tomé, A.; Vazquez-Pufleau, M.; Wagner, A.; Wanger, R.; Wang, Y.; Weitz, L.; Wimmer, D.; Wu, Y.; Yan, C.; Ye, P.; Ye, Q.; Zha, Q.; Zhou, X.; Amorim, A.; Carslaw, K.; Curtius, J.; Hansel, A.; Volkamer, R.; Winkler, P.; Flagan, R.; Kulmala, M.; Worsnop, D.; Kirkby, J.; Donahue, N.; Baltensperger, U.; El Haddad, I.; Dommen, J. The driving factors of new particle formation and growth in the polluted boundary layer. *Aerosol Sci. Technol.* **2021**, *55*, 231.

(29) Yan, C.; Nie, W.; Vogel, A. L.; Dada, L.; Lehtipalo, K.; Stolzenburg, D.; Wagner, R.; Rissanen, M. P.; Xiao, M.; Ahonen, L.; Fischer, L.; Rose, C.; Bianchi, F.; Gordon, H.; Simon, M.; Heinritzi, M.; Garmash, O.; Roldin, P.; Dias, A.; Ye, P.; Hofbauer, V.; Amorim, A.; Bauer, P. S.; Bergen, A.; Bernhammer, A. K.; Breitenlechner, M.; Brilke, S.; Buchholz, A.; Mazon, S. B.; Canagaratna, M. R.; Chen, X.; Ding, A.; Dommen, J.; Draper, D. C.; Duplissy, J.; Frege, C.; Heyn, C.; Guida, R.; Hakala, J.; Heikkinen, L.; Hoyle, C. R.; Jokinen, T.; Kangasluoma, J.; Kirkby, J.; Kontkanen, J.; Kurten, A.; Lawler, M. J.; Mai, H.; Mathot, S.; Mauldin, R. L., 3rd; Molteni, U.; Nichman, L.; Nieminen, T.; Nowak, J.; Ojdanic, A.; Onnela, A.; Pajunoja, A.; Petaja, T.; Piel, F.; Quelever, L. L. J.; Sarnela, N.; Schallhart, S.; Sengupta, K.; Sipila, M.; Tome, A.; Trostl, J.; Vaisanen, O.; Wagner, A. C.; Ylisirnio, A.; Zha, Q.; Baltensperger, U.; Carslaw, K. S.; Curtius, J.; Flagan, R. C.; Hansel, A.; Riipinen, I.; Smith, J. N.; Virtanen, A.; Winkler, P. M.; Donahue, N. M.; Kerminen, V. M.; Kulmala, M.; Ehn, M.; Worsnop, D. R. Size-dependent influence of NOx on the growth rates of organic aerosol particles. *Sci. Adv.* **2020**, *6* (22), 4945.

(30) Yan, C.; Yin, R.; Lu, Y.; Dada, L.; Yang, D.; Fu, Y.; Kontkanen, J.; Deng, C.; Garmash, O.; Ruan, J.; Baalbaki, R.; Schervish, M.; Cai, R.; Bloss, M.; Chan, T.; Chen, T.; Chen, Q.; Chen, X.; Chen, Y.; Chu, B.; Dallenbach, K.; Foreback, B.; He, X.; Heikkinen, L.; Jokinen, T.; Junninen, H.; Kangasluoma, J.; Kokkonen, T.; Kurppa, M.; Lehtipalo, K.; Li, H.; Li, H.; Li, X.; Liu, Y.; Ma, Q.; Paasonen, P.; Rantala, P.; Pileci, R. E.; Rusanen, A.; Sarnela, N.; Simonen, P.; Wang, S.; Wang, W.; Wang, Y.; Xue, M.; Yang, G.; Yao, L.; Zhou, Y.; Kujansuu, J.; Petaja, T.; Nie, W.; Ma, Y.; Ge, M.; He, H.; Donahue, N. M.; Worsnop, D. R.; Kerminen, V.-M.; Wang, L.; Liu, Y.; Zheng, J.; Kulmala, M.; Jiang, J.; Bianchi, F. The Synergistic Role of Sulfuric Acid, Bases, and Oxidized Organics Governing New-Particle Formation in Beijing. *Geophys. Res. Lett.* **2021**, *48* (7), 91944.

(31) Brean, J.; Harrison, R. M.; Shi, Z. B.; Beddows, D. C. S.; Acton, W. J. F.; Hewitt, C. N.; Squires, F. A.; Lee, J. Observations of highly oxidized molecules and particle nucleation in the atmosphere of Beijing. *Atmos. Chem. Phys.* **2019**, *19* (23), 14933−14947.

(32) Liu, Y.; Yan, C.; Feng, Z.; Zheng, F.; Fan, X.; Zhang, Y.; Li, C.; Zhou, Y.; Lin, Z.; Guo, Y.; Zhang, Y.; Ma, L.; Zhou, W.; Liu, Z.; Dada, L.; Dallenbach, K.; Kontkanen, J.; Cai, R.; Chan, T.; Chu, B.; Du, W.; Yao, L.; Wang, Y.; Cai, J.; Kangasluoma, J.; Kokkonen, T.; Kujansuu, J.; Rusanen, A.; Deng, C.; Fu, Y.; Yin, R.; Li, X.; Lu, Y.; Liu, Y.; Lian, C.; Yang, D.; Wang, W.; Ge, M.; Wang, Y.; Worsnop, D. R.; Junninen, H.; He, H.; Kerminen, V.-M.; Zheng, J.; Wang, L.; Jiang, J.; Petaja, T.; Bianchi, F.; Kulmala, M. Continuous and comprehensive atmospheric observations in Beijing: a station to understand the complex urban atmospheric environment. *Big Earth Data* **2020**, *4*, 295−321.

(33) Jokinen, T.; Sipilä, M.; Junninen, H.; Ehn, M.; Lönn, G.; Hakala, J.; Petäjä, T.; Mauldin, R. L.; Kulmala, M.; Worsnop, D. R. Atmospheric sulphuric acid and neutral cluster measurements using CI-APi-TOF. *Atmos. Chem. Phys.* **2012**, *12*, 4117−4125.

(34) Bertram, T. H.; Kimmel, J. R.; Crisp, T. A.; Ryder, O. S.; Yatavelli, R. L. N.; Thornton, J. A.; Cubison, M. J.; Gonin, M.; Worsnop, D. R. A field-deployable, chemical ionization time-of-flight mass spectrometer. *Atmos. Meas. Tech.* **2011**, *4*, 1471−1479.

(35) Heinritzi, M.; Simon, M.; Steiner, G.; Wagner, A. C.; Kürten, A.; Hansel, A.; Curtius, J. Characterization of the mass-dependent

https://doi.org/10.1021/acs.est.1c02095
Environ. Sci. Technol. 2021, 55, 13646−13656

transmission efficiency of a CIMS. *Atmos. Meas. Tech.* **2016**, *9*, 1449−1460.
(36) Cai, R.; Yan, C.; Yang, D.; Yin, R.; Lu, Y.; Deng, C.; Fu, Y.; Ruan, J.; Li, X.; Kontkanen, J.; Zhang, Q.; Kangasluoma, J.; Ma, Y.; Hao, J.; Worsnop, D. R.; Bianchi, F.; Paasonen, P.; Kerminen, V.-M.; Liu, Y.; Wang, L.; Zheng, J.; Kulmala, M.; Jiang, J. Sulfuric acid−amine nucleation in urban Beijing. *Atmos. Chem. Phys.* **2021**, *21* (4), 2457−2468.
(37) Jiang, J.; Chen, M.; Kuang, C.; Attoui, M.; McMurry, P. H. Electrical Mobility Spectrometer Using a Diethylene Glycol Condensation Particle Counter for Measurement of Aerosol Size Distributions Down to 1 nm. *Aerosol Sci. Technol.* **2011**, *45* (4), 510−521.
(38) Cai, R.; Chen, D.-R.; Hao, J.; Jiang, J. A miniature cylindrical differential mobility analyzer for sub-3 nm particle sizing. *J. Aerosol Sci.* **2017**, *106*, 111−119.
(39) Liu, J.; Jiang, J.; Zhang, Q.; Deng, J.; Hao, J. A spectrometer for measuring particle size distributions in the range of 3 nm to 10 μm. *Front. Environ. Sci. Eng.* **2016**, *10* (1), 63−72.
(40) Fu, Y.; Xue, M.; Cai, R.; Kangasluoma, J.; Jiang, J. Theoretical and experimental analysis of the core sampling method: Reducing diffusional losses in aerosol sampling line. *Aerosol Sci. Technol.* **2019**, *53*, 793−801.
(41) Cai, R.; Chen, D. R.; Hao, J.; Jiang, J. A miniature cylindrical differential mobility analyzer for sub-3 nm particle sizing. *J. Aerosol Sci.* **2017**, *106*, 111−119.
(42) Junninen, H.; Ehn, M.; Petäjä; Luosujärvi, L.; Kotiaho, T.; Kostiainen, R.; Rohner, U.; Gonin, M.; Fuhrer, K.; Kulmala, M.; Worsnop, D. R. A high-resolution mass spectrometer to measure atmospheric ion composition. *Atmos. Meas. Tech.* **2010**, *3*, 1039−1053.
(43) Kurten, A.; Rondo, L.; Ehrhart, S.; Curtius, J. Calibration of a chemical ionization mass spectrometer for the measurement of gaseous sulfuric acid. *J. Phys. Chem. A* **2012**, *116*, 6375−6386.
(44) Donahue, N. M.; Kroll, J. H.; Pandis, S. N.; Robinson, A. L. A two-dimensional volatility basis set-Part 2: Diagnostics of organic-aerosol evolution. *Atmos. Chem. Phys.* **2012**, *12*, 615−634.
(45) Wang, M.; Chen, D.; Xiao, M.; Ye, Q.; Stolzenburg, D.; Hofbauer, V.; Ye, P.; Vogel, A. L.; Mauldin, R. L., 3rd; Amorim, A.; Baccarini, A.; Baumgartner, B.; Brilke, S.; Dada, L.; Dias, A.; Duplissy, J.; Finkenzeller, H.; Garmash, O.; He, X. C.; Hoyle, C. R.; Kim, C.; Kvashnin, A.; Lehtipalo, K.; Fischer, L.; Molteni, U.; Petaja, T.; Pospisilova, V.; Quelever, L. L. J.; Rissanen, M.; Simon, M.; Tauber, C.; Tome, A.; Wagner, A. C.; Weitz, L.; Volkamer, R.; Winkler, P. M.; Kirkby, J.; Worsnop, D. R.; Kulmala, M.; Baltensperger, U.; Dommen, J.; El-Haddad, I.; Donahue, N. M. Photo-oxidation of Aromatic Hydrocarbons Produces Low-Volatility Organic Compounds. *Environ. Sci. Technol.* **2020**, *54* (13), 7911−7921.
(46) Seinfeld, J. H.; Pandis, S. N. *Atmospheric Chemistry and Physics: From Air Pollution to Cliamte Change*, 3rd ed.; John Wiley & Sons, Inc.: Hoboken, NJ, 2016.
(47) Fenelonov, V. B.; Kodenyov, G. G.; Kostrovsky, V. G. On the dependence of surface tension of liquids on the curvature of the liquid-vapor interface. *J. Phys. Chem. B* **2001**, *105*, 1050−1055.
(48) Yli-Juuti, T.; Barsanti, K.; Hildebrandt Ruiz, L.; Kieloaho, A. J.; Makkonen, U.; Petäjä, T.; Ruuskanen, T.; Kulmala, M.; Riipinen, I. Model for acid-base chemistry in nanoparticle growth (MABNAG). *Atmos. Chem. Phys.* **2013**, *13*, 12507−12524.
(49) Kulmala, M.; Petäjä, T.; Nieminen, T.; Sipilä, M.; Manninen, H. E.; Lehtipalo, K.; Dal Maso, M.; Aalto, P. P.; Junninen, H.; Paasonen, P.; Riipinen, I.; Lehtinen, K. E. J.; Laaksonen, A.; Kerminen, V. M. Measurement of the nucleation of atmospheric aerosol particles. *Nat. Protoc.* **2012**, *7*, 1651−1667.
(50) Sheng, J.; Zhao, D.; Ding, D.; Li, X.; Huang, M.; Gao, Y.; Quan, J.; Zhang, Q. Characterizing the level, photochemical reactivity, emission, and source contribution of the volatile organic compounds based on PTR-TOF-MS during winter haze period in Beijing, China. *Atmos. Res.* **2018**, *212*, 54−63.
(51) Yan, C.; Nie, W.; Äijälä, M.; Rissanen, M. P.; Canagaratna, M. R.; Massoli, P.; Junninen, H.; Jokinen, T.; Sarnela, N.; Häme, S. A. K.; Schobesberger, S.; Canonaco, F.; Yao, L.; Prévôt, A. S. H.; Petäjä, T.; Kulmala, M.; Sipilä, M.; Worsnop, D. R.; Ehn, M. Source characterization of highly oxidized multifunctional compounds in a boreal forest environment using positive matrix factorization. *Atmos. Chem. Phys.* **2016**, *16*, 12715−12731.
(52) Nieminen, T.; Lehtinen, K. E. J.; Kulmala, M. Sub-10 nm particle growth by vapor condensation-effects of vapor molecule size and particle thermal speed. *Atmos. Chem. Phys.* **2010**, *10*, 9773−9779.
(53) Rohrer, F.; Berresheim, H. Strong correlation between levels of tropospheric hydroxyl radicals and solar ultraviolet radiation. *Nature* **2006**, *442*, 184−187.
(54) Tan, Z.; Lu, K.; Hofzumahaus, A.; Fuchs, H.; Bohn, B.; Holland, F.; Liu, Y.; Rohrer, F.; Shao, M.; Sun, K.; Wu, Y.; Zeng, L.; Zhang, Y.; Zou, Q.; Kiendler-Scharr, A.; Wahner, A.; Zhang, Y. Experimental budgets of OH, HO2 and RO2 radicals and implications for ozone formation in the Pearl River Delta in China 2014. *Atmos. Chem. Phys.* **2019**, *19*, 7129−7150.
(55) Kulmala, M.; Dada, L.; Daellenbach, K. R.; Yan, C.; Stolzenburg, D.; Kontkanen, J.; Ezhova, E.; Hakala, S.; Tuovinen, S.; Kokkonen, T. V.; Kurppa, M.; Cai, R.; Zhou, Y.; Yin, R.; Baalbaki, R.; Chan, T.; Chu, B.; Deng, C.; Fu, Y.; Ge, M.; He, H.; Heikkinen, L.; Junninen, H.; Liu, Y.; Lu, Y.; Nie, W.; Rusanen, A.; Vakkari, V.; Wang, Y.; Yang, G.; Yao, L.; Zheng, J.; Kujansuu, J.; Kangasluoma, J.; Petaja, T.; Paasonen, P.; Jarvi, L.; Worsnop, D.; Ding, A.; Liu, Y.; Wang, L.; Jiang, J.; Bianchi, F.; Kerminen, V. M. Is reducing new particle formation a plausible solution to mitigate particulate air pollution in Beijing and other Chinese megacities? *Faraday Discuss.* **2021**, *226*, 334−347.
(56) Riva, M.; Rantala, P.; Krechmer, J. E.; Peräkylä, O.; Zhang, Y.; Heikkinen, L.; Garmash, O.; Yan, C.; Kulmala, M.; Worsnop, D.; Ehn, M. Evaluating the performance of five different chemical ionization techniques for detecting gaseous oxygenated organic species. *Atmos. Meas. Tech.* **2019**, *12*, 2403−2421.
(57) Ye, Q.; Wang, M.; Hofbauer, V.; Stolzenburg, D.; Chen, D.; Schervish, M.; Vogel, A.; Mauldin, R. L.; Baalbaki, R.; Brilke, S.; Dada, L.; Dias, A.; Duplissy, J.; El Haddad, I.; Finkenzeller, H.; Fischer, L.; He, X.; Kim, C.; Kürten, A.; Lamkaddam, H.; Lee, C. P.; Lehtipalo, K.; Leiminger, M.; Manninen, H. E.; Marten, R.; Mentler, B.; Partoll, E.; Petäjä, T.; Rissanen, M.; Schobesberger, S.; Schuchmann, S.; Simon, M.; Tham, Y. J.; Vazquez-Pufleau, M.; Wagner, A. C.; Wang, Y.; Wu, Y.; Xiao, M.; Baltensperger, U.; Curtius, J.; Flagan, R.; Kirkby, J.; Kulmala, M.; Volkamer, R.; Winkler, P. M.; Worsnop, D.; Donahue, N. M. Molecular Composition and Volatility of Nucleated Particles from α-Pinene Oxidation between −50°c and + 25°c. *Environ. Sci. Technol.* **2019**, *53*, 12357−12365.
(58) Olenius, T.; Yli-Juuti, T.; Elm, J.; Kontkanen, J.; Riipinen, I. Chapter 11−New Particle Formation and Growth: Creating a New Atmospheric Phase Interface. In *Physical Chemistry of Gas-Liquid Interfaces*; Faust, J. A., House, J. E., Eds.; Elsevier: Amsterdam, 2018; pp 315−352.
(59) Hallquist, M.; Wenger, J. C.; Baltensperger, U.; Rudich, Y.; Simpson, D.; Claeys, M.; Dommen, J.; Donahue, N. M.; George, C.; Goldstein, A. H.; Hamilton, J. F.; Herrmann, H.; Hoffmann, T.; Iinuma, Y.; Jang, M.; Jenkin, M. E.; Jimenez, J. L.; Kiendler-Scharr, A.; Maenhaut, W.; McFiggans, G.; Mentel, T. F.; Monod, A.; Prevot, A. S. H.; Seinfeld, J. H.; Surratt, J. D.; Szmigielski, R.; Wildt, J. The formation, properties and impact of secondary organic aerosol: current and emerging issues. *Atmos. Chem. Phys.* **2009**, *9* (14), 5155−5236.
(60) Wang, M.; Kong, W.; Marten, R.; He, X. C.; Chen, D.; Pfeifer, J.; Heitto, A.; Kontkanen, J.; Dada, L.; Kurten, A.; Yli-Juuti, T.; Manninen, H. E.; Amanatidis, S.; Amorim, A.; Baalbaki, R.; Baccarini, A.; Bell, D. M.; Bertozzi, B.; Brakling, S.; Brilke, S.; Murillo, L. C.; Chiu, R.; Chu, B.; De Menezes, L. P.; Duplissy, J.; Finkenzeller, H.; Carracedo, L. G.; Granzin, M.; Guida, R.; Hansel, A.; Hofbauer, V.; Krechmer, J.; Lehtipalo, K.; Lamkaddam, H.; Lampimaki, M.; Lee, C. P.; Makhmutov, V.; Marie, G.; Mathot, S.; Mauldin, R. L.; Mentler,

https://doi.org/10.1021/acs.est.1c02095
Environ. Sci. Technol. 2021, 55, 13646−13656

B.; Muller, T.; Onnela, A.; Partoll, E.; Petaja, T.; Philippov, M.; Pospisilova, V.; Ranjithkumar, A.; Rissanen, M.; Rorup, B.; Scholz, W.; Shen, J.; Simon, M.; Sipila, M.; Steiner, G.; Stolzenburg, D.; Tham, Y. J.; Tome, A.; Wagner, A. C.; Wang, D. S.; Wang, Y.; Weber, S. K.; Winkler, P. M.; Wlasits, P. J.; Wu, Y.; Xiao, M.; Ye, Q.; Zauner-Wieczorek, M.; Zhou, X.; Volkamer, R.; Riipinen, I.; Dommen, J.; Curtius, J.; Baltensperger, U.; Kulmala, M.; Worsnop, D. R.; Kirkby, J.; Seinfeld, J. H.; El-Haddad, I.; Flagan, R. C.; Donahue, N. M. Rapid growth of new atmospheric particles by nitric acid and ammonia condensation. *Nature* **2020**, *581* (7807), 184−189.

(61) He, X.-C.; Tham, Y. J.; Dada, L.; Wang, M.; Finkenzeller, H.; Stolzenburg, D.; Iyer, S.; Simon, M.; Kurten, A.; Shen, J.; Rorup, B.; Rissanen, M.; Schobesberger, S.; Baalbaki, R.; Wang, D. S.; Koenig, T. K.; Jokinen, T.; Sarnela, N.; Beck, L. J.; Almeida, J.; Amanatidis, S.; Amorim, A.; Ataei, F.; Baccarini, A.; Bertozzi, B.; Bianchi, F.; Brilke, S.; Caudillo, L.; Chen, D.; Chiu, R.; Chu, B.; Dias, A.; Ding, A.; Dommen, J.; Duplissy, J.; El Haddad, I.; Gonzalez Carracedo, L.; Granzin, M.; Hansel, A.; Heinritzi, M.; Hofbauer, V.; Junninen, H.; Kangasluoma, J.; Kemppainen, D.; Kim, C.; Kong, W.; Krechmer, J. E.; Kvashin, A.; Laitinen, T.; Lamkaddam, H.; Lee, C. P.; Lehtipalo, K.; Leiminger, M.; Li, Z.; Makhmutov, V.; Manninen, H. E.; Marie, G.; Marten, R.; Mathot, S.; Mauldin, R. L.; Mentler, B.; Mohler, O.; Muller, T.; Nie, W.; Onnela, A.; Petaja, T.; Pfeifer, J.; Philippov, M.; Ranjithkumar, A.; Saiz-Lopez, A.; Salma, I.; Scholz, W.; Schuchmann, S.; Schulze, B.; Steiner, G.; Stozhkov, Y.; Tauber, C.; Tome, A.; Thakur, R. C.; Vaisanen, O.; Vazquez-Pufleau, M.; Wagner, A. C.; Wang, Y.; Weber, S. K.; Winkler, P. M.; Wu, Y.; Xiao, M.; Yan, C.; Ye, Q.; Ylisirnio, A.; Zauner-Wieczorek, M.; Zha, Q.; Zhou, P.; Flagan, R. C.; Curtius, J.; Baltensperger, U.; Kulmala, M.; Kerminen, V.-M.; Kurten, T.; Donahue, N. M.; Volkamer, R.; Kirkby, J.; Worsnop, D. R.; Sipila, M. Role of iodine oxoacids in atmospheric aerosol nucleation. *Science* **2021**, *371* (6529), 589−595.

(62) Cai, R.; Li, C.; He, X.-C.; Deng, C.; Lu, Y.; Yin, R.; Yan, C.; Wang, L.; Jiang, J.; Kulmala, M.; Kangasluoma, J. Impacts of coagulation on the appearance time method for new particle growth rate evaluation and their corrections. *Atmos. Chem. Phys.* **2021**, *21* (3), 2287−2304.

(63) Zha, Q.; Yan, C.; Junninen, H.; Riva, M.; Sarnela, N.; Aalto, J.; Quéléver, L.; Schallhart, S.; Dada, L.; Heikkinen, L.; Peräkylä, O.; Zou, J.; Rose, C.; Wang, Y.; Mammarella, I.; Katul, G.; Vesala, T.; Worsnop, D. R.; Kulmala, M.; Petäjä, T.; Bianchi, F.; Ehn, M. Vertical characterization of highly oxygenated molecules (HOMs) below and above a boreal forest canopy. *Atmos. Chem. Phys.* **2018**, *18*, 17437−17450.

(64) Kürten, A.; Bergen, A.; Heinritzi, M.; Leiminger, M.; Lorenz, V.; Piel, F.; Simon, M.; Sitals, R.; Wagner, A. C.; Curtius, J. Observation of new particle formation and measurement of sulfuric acid, ammonia, amines and highly oxidized organic molecules at a rural site in central Germany. *Atmos. Chem. Phys.* **2016**, *16*, 12793−12813.

(65) Mutzel, A.; Poulain, L.; Berndt, T.; Iinuma, Y.; Rodigast, M.; Böge, O.; Richters, S.; Spindler, G.; Sipilä, M.; Jokinen, T.; Kulmala, M.; Herrmann, H. Highly Oxidized Multifunctional Organic Compounds Observed in Tropospheric Particles: A Field and Laboratory Study. *Environ. Sci. Technol.* **2015**, *49*, 7754−7761.

(66) Sarnela, N.; Jokinen, T.; Nieminen, T.; Lehtipalo, K.; Junninen, H.; Kangasluoma, J.; Hakala, J.; Taipale, R.; Schobesberger, S.; Sipilä, M.; Larnimaa, K.; Westerholm, H.; Heijari, J.; Kerminen, V. M.; Petäjä, T.; Kulmala, M. Sulphuric acid and aerosol particle production in the vicinity of an oil refinery. *Atmos. Environ.* **2015**, *119*, 156−166.

https://doi.org/10.1021/acs.est.1c02095
Environ. Sci. Technol. 2021, 55, 13646−13656